**JUSTEK : JURNAL SAINS DAN TEKNOLOGI**
http://journal.ummat.ac.id/index.php/justek
ISSN 2620-5475
Vol. 9, No. 3, September 2026, pp. 297-306

# The Effect Of Porosity On The Critical Temperature Of Porous Alumina Ceramics

**Asep Saputra[1], Parmin Lumban Toruan[2*], Atina[3]**
[1,2,3.] Physics Department, Faculty of Science and Technology, PGRI University Palembang, Indonesia
[1]asepsaputra060604@gmail.com, [2*]parmin.lt70@gmail.com , [3]atina.salsabila@gmail.com.

**ARTICLE INFO**

**Article History:**

Received : 01-07-2026
Revised : 30-08-2026
Accepted : 04-09-2026
Online : 12-09-2026

***Keywords:***
*Alumina Ceramics;*
*Porosity;*
*Critical Temperature;*
*Thermal Shock.*

**ABSTRACT**

Porous alumina ceramics are widely used in high-temperature applications due to their thermal stability; however, they are vulnerable to thermal shock, which may induce microcrack formation due to thermal stress. Although the influence of porosity on thermal shock resistance has been widely investigated, numerical studies on its effect on the critical cracking temperature remain limited. This study aims to analyze the effect of porosity on the critical temperature of porous alumina ceramics under thermal shock using a Finite Difference Method (FDM) simulation. Porosity variations of 10%, 20%, 30%, and 40% were considered. Thermal shock was modeled by applying a sudden temperature of 2000 K on one side of the material, while the initial temperature was set at 300 K. The resulting temperature distributions were used to evaluate thermal stress and determine the critical temperature for each porosity level. The results show that increasing porosity reduces the maximum thermal stress from 265 MPa at 10% porosity to 60 MPa at 40% porosity. The critical temperature increases from 533 K at 10% porosity to 663 K at 30% porosity, then decreases to 583 K at 40% porosity. These findings provide insight into the role of porosity in controlling thermal shock resistance and can support the optimization of porous alumina ceramics for high-temperature applications.



## A. INTRODUCTION

Alumina ceramic ($Al_2O_3$) is one of the engineering materials widely used in various high-temperature applications due to its thermal stability, corrosion resistance, hardness, and good electrical insulation properties (Abdelmoula et al., 2024; Hassanin et al., 2021; Sun et al., 2025; Ziva et al., 2021). This material is widely applied in refractory components, thermal insulators, high-temperature filters, and industrial components operating in extreme environments. In addition, the development of porous structures in alumina ceramics has attracted attention because it can produce lighter materials with better thermal insulation characteristics compared to dense ceramics (Shuai et al., 2024; Suleiman et al., 2022).

Although it has high thermal stability, alumina ceramics remain susceptible to thermal shock phenomena. Thermal shock occurs when a material experiences a very rapid temperature change, resulting in a large temperature gradient within the material (Gumban et al., 2023; Iqbal & Moskal, 2023; Meng et al., 2024). Temperature differences between parts of the material cause non-uniform thermal expansion and generate thermal stresses. If the resulting thermal stress exceeds the material's ability to withstand it, microcrack initiation, crack propagation, and even total material failure may occur (Iqbal & Moskal, 2023; Kamei & Khan, 2021; Liu et al., 2025). Therefore, the thermal shock phenomenon is an important factor determining the reliability of ceramics in high-temperature applications. One parameter known to influence thermal shock response is porosity. The presence of pores not only affects the thermal conductivity of the material but also influences mechanical properties such as elastic modulus and the distribution of thermal stress (Honda et al., 2022; Wen et al., 2024).

An increase in porosity generally leads to a decrease in material stiffness, so that the thermal stresses generated during the thermal shock process can be reduced. However, excessively high porosity can also reduce the mechanical strength of the material, thereby potentially decreasing the material's ability to withstand thermal loading (S. Chen et al., 2022). Thus, the effect of porosity on thermal shock behavior is a complex phenomenon that requires further study. Various studies have examined the relationship between porosity and thermal shock behavior in porous alumina ceramics. Pore characteristics are known to influence mechanical properties, thermal stress distribution, and the material's response to thermal shock loading (Honda et al., 2022). In addition, pore structure also affects residual strength and crack propagation patterns formed after the material undergoes thermal shock (M. C. Cao et al., 2021; Suleiman et al., 2022). The development of controlled porosity design has even been used to improve thermal shock performance in ceramic components produced through additive manufacturing technology (Schlacher, Geier, et al., 2024). Nevertheless, most previous studies have still focused on thermal shock resistance, post-thermal shock residual strength, and crack characteristics formed after thermal loading. Studies that specifically analyze the effect of porosity on the critical temperature of porous alumina ceramics using a numerical approach are still relatively limited (Schlacher, Geier, et al., 2024; Wei et al., 2022).

Critical temperature is an important parameter because it can be used to identify the initial condition at which indications of thermal damage appear in the material (M. Cao et al., 2021). Therefore, it is necessary to analyze the effect of porosity on the critical temperature of porous alumina ceramics using a numerical simulation based on the Finite Difference Method (FDM). The porosity variations used are 10%, 20%, 30%, and 40%, while the thermal shock condition is given by a sudden temperature of 2000 K on the left side of the material with an initial temperature of 300 K. The results of this study are expected to provide a deeper understanding of the role of porosity in determining the critical cracking temperature in porous alumina ceramics and serve as a basis for the development and optimization of ceramic material designs that are more resistant to thermal shock in high-temperature applications.

## B. METHODS

This research is a quantitative study based on numerical simulation aimed at analyzing the effect of porosity on the critical temperature of porous alumina ceramics undergoing thermal shock. The simulation is conducted using the Python programming language with the Finite Difference Method (FDM) approach. The modeling and numerical computation implemented using Python in Visual Studio Code.

**Physical Model and Material Parameters**

The material used in this study is porous alumina ceramic ($Al_2O_3$) with porosity variations of 10%, 20%, 30%, and 40%. The physical model is assumed to be a one-dimensional flat plate with a length of 10 mm (0.01 m). Under initial conditions (t=0), the entire material is at a uniform temperature of 300 K. Thermal shock conditions are applied by suddenly imposing a temperature of 2000 K on the left side of the material (x=0), while the right side of the material (x=L) is maintained at the initial temperature of 300 K. As a result of this temperature difference, heat transfer occurs by conduction from the left side toward the right side of the material.

The initial and boundary conditions used in the simulation are stated as follows:

$$T\ (x, 0) = \ 300\ K \tag{1}$$

$$T\ (0, t) = \ 2000\ K \tag{2}$$

$$T\ (L, t) = \ 300\ K \tag{3}$$

with $T$ representing temperature $(K)$, $x$ is the position along the material $(m)$, and t is the simulation time $(s)$. The thermophysical properties of the material used include density $(\rho)$, specific heat capacity $(C_p)$, thermal conductivity $(k)$, thermal expansion coefficient $(\alpha)$, elastic modulus $(E)$, and the material's flexural strength $(\sigma_f)$. The baseline parameter values of alumina used in the simulation are thermal conductivity of 25 W/m·K, density 3800 kg/m$^3$, specific heat capacity 890 J/kg·K, thermal expansion coefficient $8\ x\ 10^{-6}\ K^{-1}$, elastic modulus 340 GPa, and flexural strength 400 MPa. The effect of porosity on material properties is modeled through changes in effective thermal conductivity and effective elastic modulus, which are used as input parameters in the numerical simulation.

**Table 1.** Effective material parameters for each porosity variation

| Porositas (%) | $K_{eff}$ (W/m·K) | $E_{eff}$ (GPa) | αth (m²/s) |
|---|---|---|---|
| 10 | 22,50 | 275,40 | 6,65 x $10^{-6}$ |
| 20 | 20,00 | 217,60 | 5,92 x $10^{-6}$ |
| 30 | 17,50 | 166,60 | 5,18 x $10^{-6}$ |
| 40 | 15,00 | 122,40 | 4,44 x $10^{-6}$ |

The effective thermal conductivity (Keff), effective elastic modulus Eeff, and thermal diffusivity αth in Table 1 are obtained through empirical relationships that take into account the influence of porosity on the thermal and mechanical properties of the material. These parameters are used as inputs in numerical simulations to calculate the temperature distribution and thermal stress for each porosity variation.

**Numerical Modeling of the Finite Difference Method**

The temperature distribution within a material is calculated using the one-dimensional unsteady heat conduction equation, which is expressed as:

$$\rho C_p \frac{\partial T}{\partial t} = k \frac{\partial^2 T}{\partial x^2} \tag{4}$$

with $\rho$ representing density (kg/m$^3$), $C_p$ is specific heat (J/kg·K), $k$ is thermal conductivity (W/m·K), and $T$ is temperature (K). Equation (4) is solved using the explicit finite difference method. The material domain is divided into 100 grid points along the $x$ direction. The spacing between grid points is calculated using the equation:

$$\Delta x = \frac{L}{N_x - 1} \tag{5}$$

Where $L$ is the length of the material and $N_x$ is the number of spatial grid points. The discrete form of Equation (4) is written as:

$$T_i^{n+1} = T_i^n + Fo\,(T_{i+1}^n - 2T_i^n + T_{i-1}^n) \tag{6}$$

where $T_i^n$ is the temperature at position $i$ and time $n$, while $Fo$ is the Fourier number defined as:

$$Fo = \frac{\alpha_{th} \Delta t}{\Delta_{x^2}} \tag{7}$$

Thermal diffusivity is calculated using:

$$\alpha_{th} = \frac{k_{eff}}{\rho C_p} \tag{8}$$

The simulation was carried out using a time step of 1 × 10$^{-6}$ s with a maximum simulation time of 0.1 s. To ensure numerical stability, the following criterion is used:

$$Fo \leq 0{,}5 \tag{9}$$

These criteria are used to ensure that the numerical solution remains stable during the iteration process.

### Thermal Stress Analysis and Critical Temperature

The temperature distribution obtained from numerical simulations is used to calculate the thermal stresses formed during the thermal shock process. Thermal stress is calculated using the equation:

$$\sigma_t = E_{eff} \alpha \,(T - T_0) \tag{10}$$

where $\sigma_t$ represents thermal stress (Pa), $E_{eff}$ is the effective elastic modulus (Pa), $\alpha$ is the thermal expansion coefficient (K$^{-1}$), $T$ is the local temperature (K), and $T_0$ is the initial material temperature (300 K). The effect of porosity on thermal conductivity and elastic modulus is modeled using the following empirical relationship:

$$k_{eff} = K_0(1 - \varepsilon) \quad (11)$$

$$E_{eff} = E_0(1 - \varepsilon)^2 \quad (12)$$

with $K_0$ representing the thermal conductivity of dense alumina, $E_0$ is the elastic modulus of dense alumina, and $\varepsilon$ is the material porosity. The critical temperature is determined based on the condition when the maximum thermal stress reaches or exceeds the material's flexural strength. The criterion for determining the critical temperature is expressed as:

$$\sigma_{maks} \geq \sigma_f \quad (13)$$

with $\sigma_{maks}$ representing the maximum thermal stress calculated from the temperature distribution and $\sigma_f$ being the material's flexural strength. The determination of the critical temperature is carried out iteratively by applying variations in thermal shock temperature until a condition satisfying the Equation is obtained (Honda et al., 2022). The resulting critical temperature value is then used to evaluate the effect of porosity on porous alumina ceramics.

## C. RESULT AND DISCUSSION

### 1. Temperature Distribution Induced by Thermal Shock

The temperature distribution in porous alumina ceramics was analyzed using the Finite Difference Method (FDM) to determine the transient thermal response caused by thermal shock. The simulation began by applying a temperature of 2000 K to the left side of the material as the thermal boundary condition, with the analysis performed in one dimension. The simulation results show the evolution of the temperature distribution, which serves as the basis for the analysis of transient thermal stress. The simulated temperature distribution is shown in Figure 1.

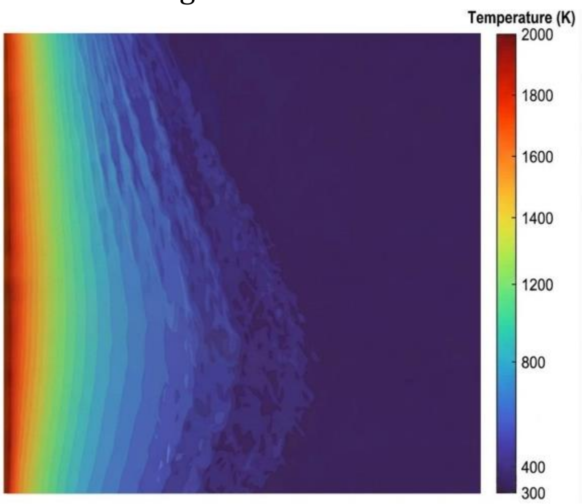


**Figure 1.** Temperature Distribution Visualization Using the FDM Method

It can be observed that the highest temperature is concentrated on the side of the material exposed to the 2000 K heat source, while the interior of the material remains at a temperature close to the initial temperature of 300 K. The color transition from red, yellow, green, to blue indicates a gradual decrease in temperature from the surface toward the interior of the material. The non-uniform temperature distribution indicates the formation of a high temperature gradient during the thermal shock process.

A temperature gradient occurs because heat is transferred through the conduction mechanism and requires time to reach all parts of the material. In porous ceramics, the presence of pores makes the heat transfer pathways discontinuous, thereby slowing the rate of heat propagation (J. Chen et al., 2024). As a result, most of the material volume remains at a relatively low temperature while the surface has already undergone significant heating. Thermal shock produces a non-uniform temperature distribution, resulting in the formation of a temperature gradient that is the primary cause of thermal stress in ceramic materials (J. Chen et al., 2024; Pang et al., 2023). This thermal heterogeneity induces localized expansion, creating differential shrinkage and internal mechanical constraints that can lead to structural failure when stresses exceed the material's fracture toughness (Garnault et al., 2021; Manière et al., 2023).

## 2. Effect of Porosity on Thermal Stress

The effect of porosity on the development of thermal stress was analyzed through the relationship between the maximum thermal stress and time at porosity levels of 10%, 20%, 30%, and 40%. Variations in porosity affect the thermomechanical characteristics of the material, thereby contributing to changes in the magnitude of the stress generated due to temperature gradients during the thermal shock process. The relationship between thermal stress and time at various porosity levels is shown in Figure 2.

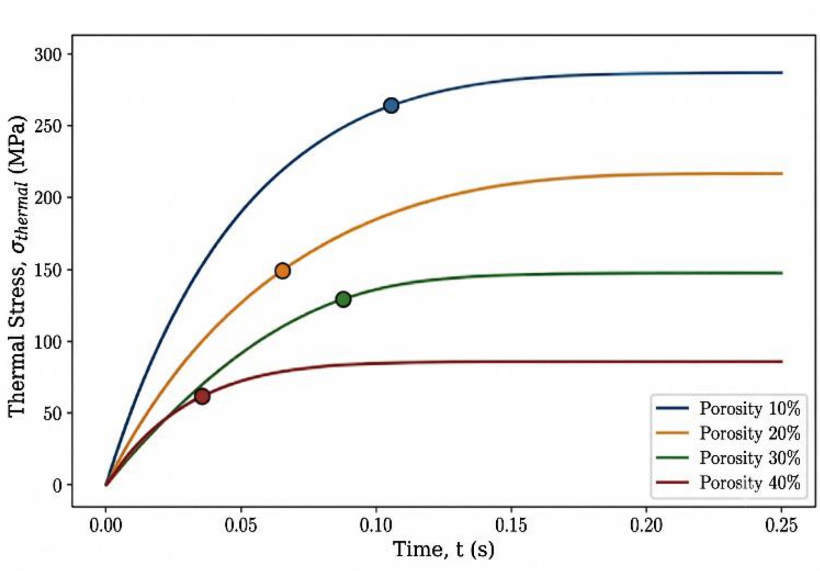


**Figure 2**. Relationship Between Thermal Stress and Time in Porous Ceramics

The simulation results show that the maximum thermal stress decreases as the material porosity increases. At 10% porosity, the maximum thermal stress reached 265 MPa at the critical time of 0.11 s. This value decreased to 150 MPa at 20% porosity, 130

MPa at 30% porosity, and 60 MPa at 40% porosity. This reduction in thermal stress indicates that the presence of pores can reduce stress accumulation caused by differences in thermal expansion within the material. Pores provide space for the material to undergo thermal deformation, thereby reducing stress concentration. In addition, increasing porosity lowers the effective elastic modulus of the material, resulting in lower thermal stress generation (Li et al., 2021). A porous structure can enhance the material's ability to relax thermal stress and inhibit crack formation caused by thermal shock (Schlacher, Mateus, et al., 2024; Shuai et al., 2024). Furthermore, while pore-induced crack deflection and arrest mechanisms contribute significantly to structural integrity (Y. Chen et al., 2021), the increased volume of pores also serves to redistribute tensile stresses more uniformly throughout the bulk of the sample (Zimina & Smolin, 2022).

### 3. The Effect of Porosity on Critical Temperature and Critical Time

The relationship between the critical temperature and the critical time with respect to variations in porosity is shown in Figure 3.

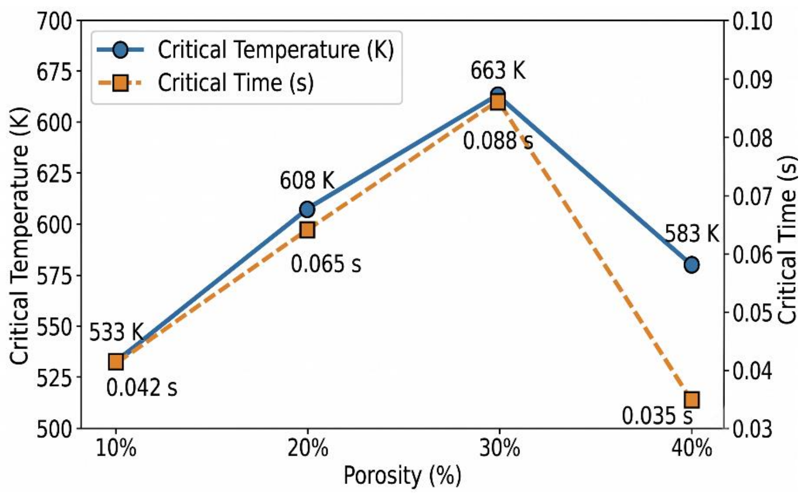


**Figure 3.** Critical Temperature versus Critical Time at Different Porosity Variations

The critical temperature increased from 533 K at 10% porosity to 608 K at 20% porosity, then reached a maximum value of 663 K at 30% porosity. However, at 40% porosity, the critical temperature decreased to 583 K. The same pattern was also observed for the critical time. The critical time increased from 0.042 s at 10% porosity to 0.065 s at 20% porosity and reached its highest value of 0.088 s at 30% porosity. Subsequently, the critical time decreased to 0.035 s at 40% porosity. The increase in critical temperature and critical time up to 30% porosity indicates that the introduction of a certain amount of pores enhances the material's resistance to thermal shock.

The presence of pores reduces the thermal stresses generated, so the material requires a higher temperature and a longer time to reach the critical condition. However, at 40% porosity, the excessive number of pores reduces the mechanical strength of the material, resulting in a decrease in thermal shock resistance. These results indicate that 30% porosity is the optimum condition within the investigated range of porosity variations. The thermal shock resistance of alumina ceramics increases up to a certain level of porosity before decreasing due to the reduced structural integrity of the material (M. Cao et al., 2021). Optimum thermal shock resistance is generally achieved within the intermediate porosity range, where the stress relaxation effect remains more dominant than the degradation of the material's mechanical strength (Han et al., 2023). This behavior occurs because pore-induced crack deflection and arrest mechanisms effectively dissipate fracture energy, a process that continues until the material surpasses a critical porosity threshold (Y. Chen et al., 2021).

## D. CONCLUSION AND SUGGESTIONS

This study successfully analyzed the effect of porosity on temperature distribution, thermal stress, and thermal shock resistance of porous alumina ceramics using the numerical simulation method, the Finite Difference Method (FDM). The simulation results showed that the thermal shock process produced a non-uniform temperature distribution, resulting in a temperature gradient that triggered the development of thermal stress within the material. Increasing the porosity from 10% to 40% caused the maximum thermal stress to decrease from 265 MPa to 60 MPa. The critical temperature, critical time, and critical temperature difference limit (ΔTcritical) increased with increasing porosity, reaching optimum values at 30% porosity, namely a critical temperature of 663 K, a critical time of 0.088 s, and a ΔTcritical of 363 K. However, at 40% porosity, the thermal shock resistance decreased due to the reduced mechanical strength of the material. Therefore, porosity has a significant effect on the thermal shock resistance of porous alumina ceramics, and a porosity of 30% represents the optimum condition within the range of variations investigated.

To strengthen the direction of this research and support its future development potential, several recommendations are proposed. Future studies are encouraged to develop simulation models that consider more complex pore geometries and non-uniform pore distributions in order to better represent actual material conditions. In addition, the simulation results should be validated through experimental thermal shock testing on porous alumina ceramics so that the accuracy of the model can be evaluated more comprehensively. Further research may also investigate the effects of pore size, pore shape, and variations in heating and cooling rates on thermal shock resistance to achieve a deeper understanding of the thermomechanical behavior of porous ceramics in high-temperature applications.

## REFERENCES

Abdelmoula, M., Küçüktürk, G., Juste, E., & Petit, F. (2024). Enhancing powder bed fusion of alumina ceramic material: a comprehensive study from powder tailoring to mechanical performance evaluation. *The International Journal of Advanced Manufacturing Technology*, *131*(3), 1745–1767. https://doi.org/10.1007/s00170-024-13158-x

Cao, M. C., Jin, X. X., Dong, L. M., Li, X. Y., & Zhang, X. Y. (2021). *Effect of Pore Composition on Thermal Shock Resistance of Porous Ceramics*. *16*(1), 1–9. https://doi.org/10.15251/DJNB.2021.161.1

Cao, M., Jin, X., Chen, L., Dong, L., Li, B., & Zhang, X. (2021). Thermal shock resistance of porous alumina ceramics with different internal and external porosity. *Journal of Ceramic Processing Research*, *22*(4), 377–385. https://doi.org/10.36410/jcpr.2021.22.4.377

Chen, J., Ke, J., Zhou, J., Jiao, Z., Zhong, Z., & Zhang, J. (2024). Grain boundary effects on thermal shock responses of yttria-stabilized zirconia. *International Journal of Mechanical Sciences*,

*266*, 108950. https://doi.org/10.1016/j.ijmecsci.2023.108950
Chen, S., Wang, L., He, G., Li, J., & Wang, C.-A. (2022). Microstructure and properties of porous Si3N4 ceramics by gelcasting-self-propagating high-temperature synthesis (SHS). *Journal of Advanced Ceramics*, *11*(1), 172–183. https://doi.org/10.1007/s40145-021-0525-7

Chen, Y., Wang, N., Ola, O., Xia, Y., & Zhu, Y. (2021). Porous ceramics: Light in weight but heavy in energy and environment technologies. *Materials Science and Engineering: R: Reports*, *143*, 100589. https://doi.org/10.1016/j.mser.2020.100589

Garnault, T., Bouvard, D., Chaix, J.-M., Marinel, S., & Harnois, C. (2021). Is direct microwave heating well suited for sintering ceramics? *Ceramics International*, *47*(12), 16716–16729. https://doi.org/10.1016/j.ceramint.2021.02.242

Gumban, C. G., Hubálková, J., Neumann, M., Werzner, E., Charitos, A., Aneziris, C. G., & Voigt, C. (2023). Thermal shock resistance of industrial foam filters-a comparative study. *Open Ceramics*, *16*, 100463. https://doi.org/10.1016/j.oceram.2023.100463

Han, J., Liu, C., Bradford-Vialva, R. L., Klosterman, D. A., & Cao, L. (2023). Additive Manufacturing of Advanced Ceramics Using Preceramic Polymers. *Materials*, *16*(13), 4636. https://doi.org/10.3390/ma16134636

Hassanin, H., Essa, K., Elshaer, A., Imbaby, M., El-Mongy, H. H., & El-Sayed, T. A. (2021). Micro-fabrication of ceramics: Additive manufacturing and conventional technologies. *Journal of Advanced Ceramics*, *10*(1), 1–27. https://doi.org/10.1007/s40145-020-0422-5

Honda, S., Hashimoto, S., Nait-Ali, B., Smith, D. S., Daiko, Y., & Iwamoto, Y. (2022). Characterization of anisotropic gas permeability and thermomechanical properties of highly textured porous alumina. *Journal of the American Ceramic Society*, *105*(10), 6335–6344. https://doi.org/10.1111/jace.18573

Iqbal, A., & Moskal, G. (2023). Recent Development in Advance Ceramic Materials and Understanding the Mechanisms of Thermal Barrier Coatings Degradation. *Archives of Computational Methods in Engineering*, *30*(8), 4855–4896. https://doi.org/10.1007/s11831-023-09960-7

Kamei, K., & Khan, M. A. (2021). Current challenges in modelling vibrational fatigue and fracture of structures: a review. *Journal of the Brazilian Society of Mechanical Sciences and Engineering*, *43*(2), 77. https://doi.org/10.1007/s40430-020-02777-6

Li, B., Yan, Y., Jin, X., Geng, Y., Wang, S., Cao, M., He, X., Li, N., & Zhuang, Y. (2021). Microstructure and mechanical and thermal shock properties of hierarchically porous ceramics. *Ceramics International*, *47*(17), 24887–24894. https://doi.org/10.1016/j.ceramint.2021.05.215

Liu, K., Lv, D., Du, Y., Ye, G., Wang, Y., Fan, W., Zhang, L., & Cao, Y. (2025). Study on multimodal crack growth of FG-TBCs and its influence on interface cracking. *Journal of Materials Research and Technology*, *36*, 8920–8934. https://doi.org/10.1016/j.jmrt.2025.05.108

Manière, C., Harnois, C., Riquet, G., Grippi, T., Behar-Lafenetre, S., & Marinel, S. (2023). Rapid microwave sintering of centimetric zirconia: Scalability and electromagnetic-thermal-fluid-dynamic simulation. *Journal of the American Ceramic Society*, *106*(2), 848–859. https://doi.org/10.1111/jace.18787

Meng, Q., Zhang, K., He, R., & Qu, Z. (2024). A review of thermal shock behavior of ceramics: Fundamental theory, experimental methods, and outlooks. *International Journal of Applied Ceramic Technology*, *21*(6), 3789–3811. https://doi.org/10.1111/ijac.14846

Pang, Y., Li, D., Li, X., Wang, R., & Ao, X. (2023). Phase-Field Simulation of Temperature-Dependent Thermal Shock Fracture of Al2O3/ZrO2 Multilayer Ceramics with Phase Transition Residual Stress. *Materials*, *16*(2). https://doi.org/10.3390/ma16020734

Schlacher, J., Geier, S., Schwentenwein, M., & Bermejo, R. (2024). Towards 3D-printed alumina-based multi-material components with enhanced thermal shock resistance. *Journal of the European Ceramic Society*, *44*(4), 2294–2303. https://doi.org/10.1016/j.jeurceramsoc.2023.11.009

Schlacher, J., Mateus, L. B., Nohut, S., Schwentenwein, M., & Bermejo, R. (2024). Thermal shock resistant 3D-printed ceramic components through spatially tailored porosity. *Additive Manufacturing*, *96*, 104582. https://doi.org/10.1016/j.addma.2024.104582

Shuai, Y., Ai, J., Hu, L., Xu, H., Cheng, L., Chen, Z., Zhou, Z., & Li, W. (2024). Residual strength of porous alumina ceramics and fractal characterization of their crack patterns after thermal shocks. *Ceramics International*, *50*(21, Part A), 41848–41856. https://doi.org/10.1016/j.ceramint.2024.08.038

Suleiman, B., Zhang, H., Ding, Y., & Li, Y. (2022). Microstructure and mechanical properties of cold sintered porous alumina ceramics. *Ceramics International*, *48*(10), 13531–13540. https://doi.org/10.1016/j.ceramint.2022.01.232

Sun, Y., Li, S., Zhao, Q., Cong, Z., Xia, Y., jiao, X., & Chen, D. (2025). Recent Advancements in Alumina-Based High-Temperature Insulating Materials: Properties, Applications, and Future Perspectives. *High-Temperature Materials*, *2*(1), 10001–10001. https://doi.org/10.70322/htm.2025.10001

Wei, Z.-Y., Meng, G.-H., Chen, L., Li, G.-R., Liu, M.-J., Zhang, W.-X., Zhao, L.-N., Zhang, Q., Zhang, X.-D., Wan, C.-L., Qu, Z.-X., Chen, L., Feng, J., Liu, L., Dong, H., Bao, Z.-B., Zhao, X.-F., Zhang, X.-F., Guo, L., … Li, C.-J. (2022). Progress in ceramic materials and structure design toward advanced thermal barrier coatings. *Journal of Advanced Ceramics*, *11*(7), 985–1068. https://doi.org/10.1007/s40145-022-0581-7

Wen, Z., Tang, Z., Liu, Y., Zhuang, L., Yu, H., & Chu, Y. (2024). Ultrastrong and High Thermal Insulating Porous High-Entropy Ceramics up to 2000 °C. *Advanced Materials*, *36*(14), 2311870. https://doi.org/10.1002/adma.202311870

Zimina, V. A., & Smolin, I. Y. (2022). Features of the stress state of porous brittle materials under tensile conditions. *Diagnostics, Resource and Mechanics of Materials and Structures*, *2*, 35–44. https://doi.org/10.17804/2410-9908.2022.2.035-044

Ziva, A. Z., Suryana, Y. K., Kurniadianti, Y. S., Nandiyanto, A. B. D., & Kurniawan, T. (2021). Recent Progress on the Production of Aluminum Oxide (Al2O3) Nanoparticles: A Review. *Mechanical Engineering for Society and Industry*, *1*(2), 54–77. https://doi.org/10.31603/mesi.5493